The 2010 IEEE/RSJ International Conference on
Intelligent Robots and Systems
October 18-22, 2010, Taipei, Taiwan

Embedding Range Information in Omnidirectional Images through Laser Range Finder

E.B. Bacca, E. Mouaddib, X. Cufí

Abstract— **Robot map navigation and localization are challenging tasks that require the solving of the data association problem for local and global features. Data fusion allows the advantages of two or more sensors to be combined, and complementary cooperation can be obtained. This paper presents two methods to embed depth information in omnidirectional images using the extrinsic calibration of a 2D laser range finder and a central catadioptric camera. The methods presented do not require a visible laser beam, but they assume the planar checkerboard patterns are visible for both the catadioptric camera and the 2D laser range finder. Unlike other approaches, the methods proposed used an invisible laser trace, and they are evaluated at pixel error level using ground truth data from the calibration patterns projected in the omnidirectional image. Results include a mean square error analysis of all calibration poses, and laser point projection on indoor omnidirectional images. We think that embedding range information in omnidirectional images is an interesting tool for data fusion approaches, which can be used in robot map building and localization.**

I. Introduction

OVER many years, 2D laser range finders (LRFs) have been a basic tool in robot navigation and mapping. During this time, machine vision techniques based on one or more perspective cameras have been used in order to solve the SLAM (Simultaneous Localization and Mapping) problem. Omnidirectional vision is now receiving special attention due to its long-term landmark tracking, reduced perceptual aliasing, and robustness to occlusions. Omnidirectional images and 2D LRF data have a higher capability of exploiting their wide field of view compared with the setup of a perspective camera and a LRF. An interesting sensor setup composed by a catadioptric central camera and a 2D LRF could be useful in service robots for surveillance, inspection, delivery, cleaning and exploration tasks which mostly use appearance-based maps.

Our main goal is to embed range information in omnidirectional images. To do this we use the extrinsic calibration of a 2D LRF and a catadioptric camera, which can be used for data fusion in mobile robot applications. The calibration of a camera, either perspective or catadioptric, and a 2D [1-5] or 3D [6-10] LRF is not a new issue but few works show detailed information using a catadioptric sensor and an LRF. A state of art about the extrinsic calibration of these sensors is shown in Table 1. Works such as [5] report interesting methods for visible laser traces, but this approach clearly cannot be applied to a 2D LRF with an invisible trace as mostly used in robotics (SICK or HOKUYO). Other works like [8] and [9] build a minimization function based on the re-projection error, or obtain a closed form solution based on conics, since they use visible laser traces but their results show they have a limited range of operation. 2D LRFs are commonly used to build 3D range scans by adding a pan/tilt mechanism. This is the case with [7], where a 3D range scan and a catadioptric camera are used in 3D indoor/outdoor environmental reconstruction adopting a camera/laser calibration based on [10], which does not reveal enough details of the calibration process. In terms of perspective cameras, [3] has a general non-linear approach unlike [1]. The method proposed in [3] can be extended to omnidirectional cameras, and the methods of this paper are based on that approach. A Matlab toolbox is included in [6], but does not give enough details of its model.

TABLE I
State of art summary for LRF and camera calibration

Ref.	Sensors	Observation
[1]	Persp. Cam. + 2D LRF	Calibration using linear models.
[3]	Persp. Cam. + 2D LRF	Adaptable to central catadioptric cameras
[4]	Persp. Cam. + 2D LRF	Calibration based on specific target
[5]	Omni. Cam. + 2D LRF (visible, invisible)	Several methods for visible laser, but not clear for invisible laser
[6]	Persp. Cam. + 3D LRF	Fast calibration using a Matlab toolbox
[7]	Omni. Cam. + 3D LRF	One shot calibration
[8-9]	Omni. Cam. + 2D LRF (visible)	Closed solution based on conics.
[10]	Persp. Cam. + 3D LRF	Not enough details about calibration

It is important to differentiate our work from the works in Table I. These use catadioptric cameras and a 2D laser with approaches applicable to visible laser traces. Other works use perspective cameras and a 2D LRF, with results that are adaptable to the catadioptric cameras case. Our approach embeds range information in omnidirectional images using

Manuscript received October 9, 2001. This work is partially supported by LASPAU-COLCIENCIAS grant 136-2008, Universidad del Valle-Cali-Colombia contract No. 644-19-04-95, the VICOROB research group, the Doctoral Program in Technologies at the University of Girona, Spain, and the Commission of Science and Technology of Spain (CICYT) through coordinated project DPI-2007-66796-C03-02

E. B. Bacca is a Ph.D. student at the University of Girona, Girona, 17071, Spain, and an assistant professor at the Universidad del Valle, Cali, Colombia (corresponding author: +34 972-418486; fax: +34 972-418976; e-mail: bladimir@eia.udg.edu, evbacca@univalle.edu.co).

E. Mouaddib, is with research lab of Modélisation, Information et Systèmes, Université de Picardie Jules Verne, 80039 Amiens, France (e-mail: mouaddib@u-picardie.fr).

X. Cufí, is with research group VICOROB and the Department of Electronic, Computer Science and Automatic Engineering, University of Girona, Girona, 17071, Spain, (e-mail: xcuf@eia.udg.edu).

the extrinsic calibration of a 2D LRF with an invisible laser trace and an omnidirectional camera using checkerboard patterns, and laser data points on these patterns. Unlike [3] or [5], we propose two calibration methods and three initial guess options. The calibration methods proposed are evaluated at pixel error level using ground truth data from the calibration patterns projected onto the omnidirectional image. This error analysis is useful for data fusion approaches in mobile robotics localization, mapping and navigation. In this work, the omnidirectional camera was calibrated with the C. Mei toolbox [11], and the 2D LRF with invisible trace was calibrated following the procedure specified in [12-13]. According to the review of our state of art, the calibration between an omnidirectional camera and a 2D LRF with invisible trace has not been published with the level of detail presented in this paper, which does not allow us to compare to other similar methods.

The remainder of this paper is organized as follows: Section 2 describes the LRF calibration, two approaches for obtaining the extrinsic laser/camera parameters are presented in Section 3, Section 4 shows the experiments and results, and Section 5 presents our conclusions.

II. LASER RANGE FINDER CALIBRATION

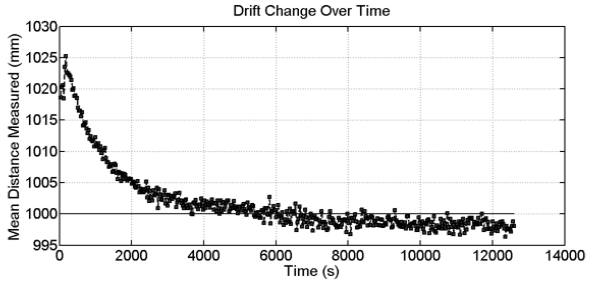

Fig. 1. LRF drift effect over time.

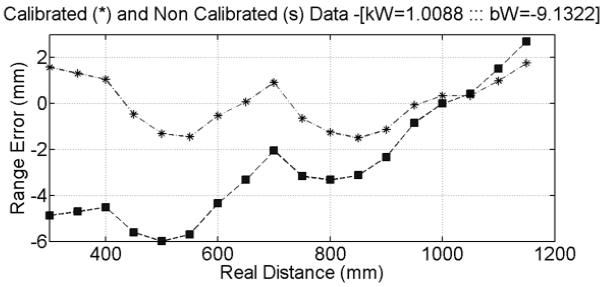

Fig. 2. Range error vs. real distance of calibrated (top) and non-calibrated (bottom) laser readings.

The literature offers few works exploring systematic errors of the LRF despite the fact that LRFs are commonly used in robotics. A good characterization of these sensors is shown in [12] and [13] exploring additional characteristics like: laser alignment, drift effect and laser model. We collected the suggestions about the material properties described in [12] and [13] in order to decrease the range error. We use the URG-04LX LRF, and the results we achieved were in accordance with [14].

Range fluctuations can be present in the LRF at power-up. Following the methodology mentioned in [13], we got Fig. 1 which shows that after 90minutes the range measure was stable. From then on, for data acquisition in this work the laser was turned on 90minutes before first use. We found a linear trend between the real distance and the mean at each position, which agrees with [12], [13] and [14]. After running 10 different tests, we found the following laser range model: $d = 1.0088l - 9.1322$, where: l is the range given by the LRF, and d is the estimated range. Fig. 2 shows the range error $\bar{y} - y$, or the difference between the estimated distance and real distance, vs. the real distance.

III. 2D LASER RANGE FINDER AND CENTRAL CATADIOPTRIC CAMERA CALIBRATION METHODS

A central catadioptric camera consists of a perspective or orthographic camera, and a mirror. The latter can be conic, hyperbolic, or parabolic. Projective models for these cameras have been developed by [15], [16] and [17]. In the remainder of this paper we adopt the model described in [17], which is related to the toolbox described in [11], and use it to calibrate our central catadioptric camera.

The LRF readings are distance measurements, belonging to a 2D plane parallel to the floor. We use a coordinate system where the Z axis points upwards, the Y axis points forward, and is centered on the laser projection point. This is the same axis configuration as for the catadioptric camera, but centered on the mirror's central projection point.

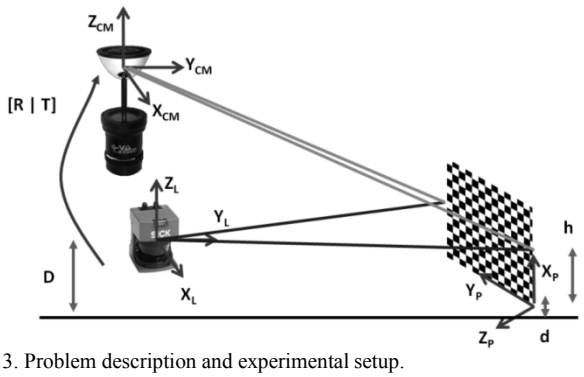

Fig. 3. Problem description and experimental setup.

Fig. 3 shows our main goal and experimental setup. There are three coordinate systems, those of the laser, the calibration pattern and the camera. Our problem focuses on finding R and T so that laser points P_L can be represented in the camera coordinate system, and then projected onto the omnidirectional image. Zhang and Pless [3] base their model finding a rotation matrix R and a translation vector T in a simultaneous manner, our approach finds R and T through a simultaneous and non-simultaneous way, and we explore three different methods to get the initial guess for the non-linear minimization. A point P_C in the camera coordinate frame can be described by (1).

$$P_C = RP_L + T \quad (1)$$

Where, P_L is a point in the laser coordinate frame, R is a

3x3 rotation matrix, and T is a 3D translation vector of the camera center of projection with respect to the laser frame. Our goal is to find R and T using the checkerboard planes, which are visible from the laser and camera point of view. This paper shows two methods to find R and T. The first, which tries to find them simultaneously performing two non-linear minimization processes, it has the advantage of arriving at a solution regardless of any alignment constraint between the LRF and the omnidirectional camera, but it involves 6 degrees of freedom (DOF) estimation. The second tries to find the translation vector T, and then the rotation matrix R. This decoupled parameter estimation has the advantage to reduce the problem estimation to 3DOF + 3DOF, which requires less training data in comparison with a simultaneous parameter estimation. In both cases a Levenberg-Marquardt (LM) optimization algorithm was used because it is easy to implement, it generally has a fast convergence rate, and we think that it is sufficient for our approach. However, this algorithm is sensitive to the initial guess [18]. Then, three different ways to calculate this initial guess were implemented and the results processed using [19].

A. Methods to Obtain the Initial Guess

We implemented three different methods to get the initial guess for the LM optimization algorithm, which differs from [3]. First, we selected one of the calibration poses available and a set of linear least squares (LLS) equations were defined using these laser points. Second, we selected two calibration poses and the LLS equations were defined using these points. And third, we used a sub-set of the central laser points of each calibration pose to build the LLS equations.

B. Simultaneous Parameter Estimation

Data acquisition for this method includes images with checkerboard calibration planes and 2D laser points which belong to the calibration plane. Using these images camera calibration was performed and the extrinsic parameters were then used to define a vector parallel to the normal calibration plane as described by (2) [3].

$$N_C = R_{3W}(R_{3W}^T . T_W) \tag{2}$$

Where, R_{3W} and T_W are the third column of the rotational matrix and the translation vector of the calibration plane pose with respect to the omnidirectional camera. Since, the laser points belong to the calibration plane there is a geometric constraint based on the distance between the camera and the calibration plane. This constraint can be expressed by (3) [3].

$$N_C . (RP_L + T) = \|N_C\|^2 \tag{3}$$

Where, R and T are the parameters to estimate, and P_L is a laser point. This expression differs from that proposed in [3] since we are working in the camera frame rather than the laser frame. Using (3) a non-linear minimization function can be expressed as in (4) and (5).

$$f(R,T,P_L) = N_C . (RP_L + T) - \|N_C\|^2 \tag{4}$$

$$\nabla_{Q,T} f(R,T,P_L) = N_C . \left[\nabla R_{Q,P_L} \nabla n_Q,\ I_{3x3}\right] \tag{5}$$

Where, $\nabla_{Q,T} f(R,T,P_L)P_L$ is the gradient of the minimization function using quaternions instead rotational matrix, $\nabla R_{Q,P_L}$ is the quaternion's gradient evaluated at point P_L, and ∇n_Q is the gradient of the quaternion's normalization factor. A LM algorithm was used to minimize (4), and we described three different ways to obtain the initial guess. By organizing the laser points in an AX=B system, and using (4), the LLS equations we got for the initial guess are (6), (7) and (8).

$$[N_{CX}P_{LX}, N_{CX}P_{LY}, N_{CX}P_{LZ}, N_{CY}P_{LX}, N_{CY}P_{LY}, N_{CY}P_{LZ}, N_{CZ}P_{LX} \; N_{CZ}P_{LY}, N_{CZ}P_{LZ}, N_{CX}, N_{CY}, N_{CZ}] = A_i \tag{6}$$

$$\left[r_{11}, r_{12}, r_{13}, r_{21}, r_{22}, r_{23}, r_{31}, r_{32}, r_{33}, t_x, t_y, t_z\right]^T = X \tag{7}$$

$$\|N_C\|^2 = B_i \tag{8}$$

Where, A_i is a row of the A matrix, B_i is a row of the B vector, X is the vector parameters to estimate, N_{CX}, N_{CY} and N_{CZ} are the N_C vector components of (2), r_{11} to r_{33} are the 9 terms of the rotation matrix, t_x, t_y and t_z are the translation vector, and P_{LX}, P_{LY} and P_{LZ} are the *i-th* laser point components. The solution to these simultaneous equations gives a rank-2 rotation matrix for all three methods to obtain the initial guess. This happens when the training points are planar [19] like the laser points, which are constrained to a 2D plane parallel to the floor. Due to this, the resulting matrix is not a proper rotation matrix, since it does not satisfy $RR^T = I$. In order to resolve this problem, Eggert et. al. [19] propose finding the nearest rotation matrix which satisfies $RR^T = I$, by calculating the eigen-values and eigen-vectors of the resulting matrix, the nearest proper rotation matrix can be expressed by (9).

$$\hat{R} = MS^+ \pm \frac{X}{\sqrt{|Trace(X)|}} \tag{9}$$

$$S^+ = \left(\frac{u_1 u_1^T}{\sqrt{\delta_1}} + \frac{u_2 u_2^T}{\sqrt{\delta_2}}\right) \tag{10}$$

$$X = [(MS^+)(MS^+)^T - I]u_3 u_3{}^T \tag{11}$$

Where, u_1 and u_2 are the eigen-vectors corresponding to the non-zero eigen-values δ_1 and δ_2, and u_3 is the eigen-vector associated with the zero eigen-value. The sign in (9) is chosen in line with the determinant of $\hat{R}$ being +1; and M is the LLS resulting matrix. After the LLS and the first non-linear minimization are solved, a second non-linear minimization is performed using and Euclidean constraint rather than a geometrical one. This is shown in (12).

$$f(R,T,P_L) = \sum_{i=1}^{K} \sum_{j=1}^{M} \frac{1}{2}\left(\frac{N_{Ci}}{\|N_{Ci}\|}\left(RP_{Lij} + T\right) - \|N_{Ci}\|\right) \tag{12}$$

Where, K is the total number of calibration poses, M is the

total number of laser points in the *i-th* checkerboard pattern, and N_{Ci} is the vector defined by (5) for the *i-th* calibration plane. The minimization algorithm used was LM, but with an initial guess given by the first minimization stage.

C. Non-Simultaneous Parameter Estimation

Our second approach consists of performing a decoupled parameter estimation. First, the translation vector is found, and then the rotation matrix is estimated using this information. This decoupled problem statement is common in mobile robotics [6], [11]. In general, this method uses the same minimization and geometrical constraints as above. In the translation vector estimation (2) to (4) are still valid. But, the Jacobian is now described by (13). The initial guess for the LM algorithm can be re-written as shown in (14) to (16).

$$\nabla_{Q,T} f(R,T,P_L) = N_C.[I_{3x3}] \quad (13)$$

$$[N_{CX}\ N_{CY}\ N_{CZ}] = A_i \quad (14)$$

$$[t_x\ t_y\ t_z]^T = X \quad (15)$$

$$\|N_C\|^2 - (N_{CX}P_{LX} + N_{CY}P_{LY} + N_{CZ}P_{LZ}) = B_i \quad (16)$$

Where, A_i is a row of the A matrix, B_i is a row of the B vector, X is the parameters to estimate, N_{CX}, N_{CY} and N_{CZ} are the N_C vector components of (2), t_x, t_y and t_z are the translation vector, and P_{LX}, P_{LY} and P_{LZ} are the *i-th* laser point components. The second parameter estimation calculates the rotation matrix using the translation vector found above. Equations (2) to (4) are still valid, but their Jacobian is described by (17). The initial guess of the rotation matrix changes too, and the LLS equations can then be expressed as shown (18) to (20).

$$\nabla_{Q,T} f(R,T,P_L) = N_C.\left[\nabla R_{Q,P_L} \nabla n_Q\right] \quad (17)$$

$$[N_{CX}P_{LX}, N_{CX}P_{LY}, N_{CX}P_{LZ}, N_{CY}P_{LX}, N_{CY}P_{LY}, N_{CY}P_{LZ}, N_{CZ}P_{LX}, N_{CZ}P_{LY}, N_{CZ}P_{LZ}, N_{CX}, N_{CY}, N_{CZ}] = A_i \quad (18)$$

$$[r_{11}, r_{12}, r_{13}, r_{21}, r_{22}, r_{23}, r_{31}, r_{32}, r_{33}]^T = X \quad (19)$$

$$\|N_C\|^2 - (N_{CX}T_X + N_{CY}T_Y + N_{CZ}T_Z) = B_i \quad (20)$$

Where, A_i is a row of the A matrix, B_i is a row of the B vector, X is the vector parameters to estimate, N_{CX}, N_{CY} and N_{CZ} are the N_C vector components of (2), r_{11} to r_{33} are the 9 terms of the rotation matrix, P_{LX}, P_{LY} and P_{LZ} are the *i-th* laser point components, and T_X, T_Y and T_Z are the translation vector components of the first minimization stage. The resulting rotation matrix has the same rank-2 problem as described previously, so the nearest proper rotation matrix is found following the same procedure as shown above. In similar way as the simultaneous parameter estimation, a second minimization is performed using (12).

IV. EXPERIMENTS AND RESULTS

Four sets of images were used to validate the methods proposed. Each set contained 16 images and the same number of laser points. The main difference between the sets was the environment structure, which was used to show the usefulness of our method. The data acquisition process had 6 main steps: first, laser alignment was performed; second, there was a warm-up period of 90minutes; third, the checkerboard calibration pattern was placed; fourth, 15 laser readings were taken and corrected according to the laser model; fifth, an omnidirectional image was captured; sixth, steps 3 to 5 were repeated until acquisition was completed. The omnidirectional camera was calibrated, and its intrinsic and extrinsic parameters were used to get the "ground truth" of the laser points on the calibration planes only. We know that it is difficult to get a reliable ground truth data. However, taking advantage of our experimental setup (Fig. 3), we can define: $h = D - d$, where D is the distance from the laser to the floor, d is the distance from the bottom right corner on the calibration pattern to the floor, and h is the relative distance from the laser trace to the calibration pattern origin. D and d were measured with a LLB-60D laser (±1.5mm). Then, using the intrinsic and extrinsic camera parameters a very close "ground truth" data can be obtained. In this way, unlike with [3] and [5] we were able to get the pixel error associated to the laser point's projection onto the omnidirectional image. Using the ground truth and the experimental laser points projected onto the omnidirectional image, the results for the three initial guess methods were tested. Finally, the calibration planes were taken out, and LRF readings were projected onto the omnidirectional image, showing depth perception on these images.

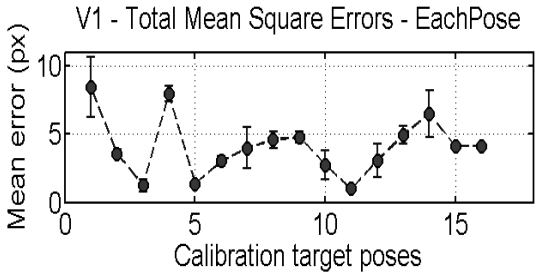

Fig. 4 Results for simultaneous estimation with a total MSEs less than 5px over all poses and an initial guess using a single calibration pose.

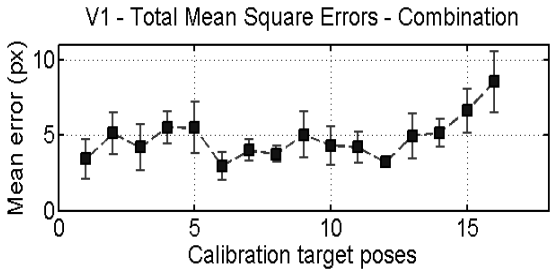

Fig. 5 Results for simultaneous estimation with a total MSE less than 5px over all poses, and an initial guess using two calibration poses.

Using the four sets of calibration images a total of 298 calibration results were processed, 50% for the simultaneous (V1) and another 50% for the non-simultaneous (V2) estimation. From these calibration results only those with a total MSE error less than 5px obtained considering all calibration poses were considered and classified by the

initial guess method used. The graphs of this MSE error vs. calibration target poses are plotted in Fig. 4 to 7. Fig. 4 and 5 show results for simultaneous parameter estimation. These figures show initial guess methods corresponding to take one calibration plane, and to take two calibration planes to build the LLS equations. It should be noted that the initial guess method which takes the central points of all the calibration planes is not present. Even so, the calibration results show that if a total MSE less than 10px is considered only one result is found for this initial guess method. To build Fig. 4 and 5 a total of 20 and 40 calibration results were considered for these initial guess methods. Using these results, their error bands are plotted using a T-Student distribution with a confidence of 97.5%. Clearly, if two calibration poses are used as initial guess, is more likely to get a solution with less MSE error in comparison to use one calibration plane. However, Fig. 4 shows some errors go closer to 0; in this case an option would be run many times this method using this initial guess and choose the best answer.

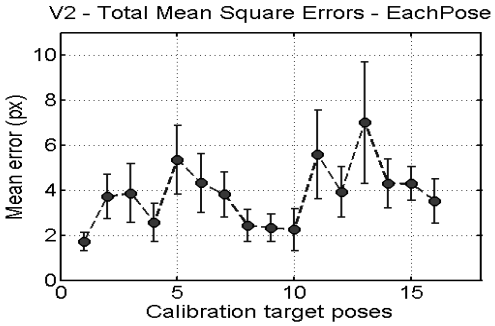

Fig. 6 Results for non-simultaneous estimation with a total MSEs less than 5px over all poses, and an initial guess using a single calibration pose.

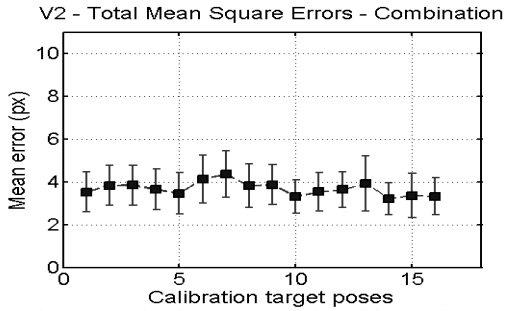

Fig. 7 Results for non-simultaneous estimation with a total MSEs less than 5px over all poses, and an initial guess using two calibration poses.

Fig. 6 and 7 show similar results for non-simultaneous parameter estimation. Again, the initial guess method which takes the central points of all calibration planes is not present. In this case, even with a total MSE of less than 20px (extremely high and with no practical use) it was not possible to obtain any calibration result with this initial guess method. To build Fig. 6 and 7 a total of 30 and 119 calibration results for these initial guess methods were considered and the same distribution and confidence band were used. It can be observed that in the cases of both simultaneous and non-simultaneous estimation, the combination of calibration planes obtains more homogeneous results in error data plots, than the initial guess method which uses only one calibration plane. Simultaneous parameter estimation has less chance to get successful results than non-simultaneous estimation using our data set, because in the first case the degrees of freedom within each minimization are more than in the second case. However, Fig. 6 shows 5 excellent calibration results close to 2px, but 4 with MSE greater than 4px and wide confidence bands.

Amongst these 4 data sets, we can see that noisy laser readings can cause a loss of calibration accuracy, making difficult to get a good enough initial guess due its geometrical constraint, which matches with assumptions made in [6]. Another problem that was found related to the relative position of the calibration plane with respect to the LRF, since if the calibration plane is placed vertically along the Y axis in relation to the laser and camera, then not enough and not accurate laser readings are available.

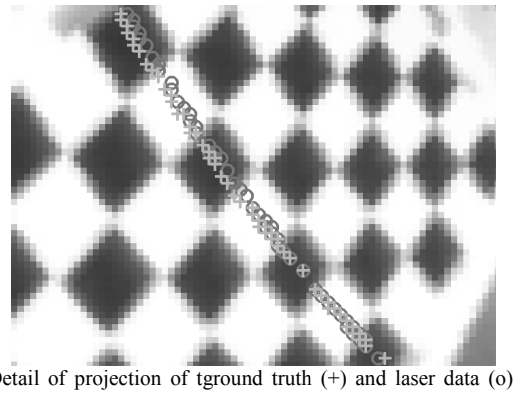

Fig. 8 Detail of projection of tground truth (+) and laser data (o) onto a calibration pattern.

Fig. 8 shows the laser points (o) projected onto the omnidirectional image as well as our ground truth (+). This figure shows a zoomed portion of the omnidirectional image, though for space reasons the complete omnidirectional image is not shown. An important thing should be noted, there are some missing laser readings on the black squares at bottom right of Fig. 8, which are due to the relative orientation between the calibration plane and the LRF, and because the URG-04LX LRF is a low power device.

Embedding range information onto omnidirectional images can be useful when trying to perform a sensor data fusion, in this case of a catadioptric camera and an LRF. The usefulness of this data fusion can be exploited using the scene vertical lines, which are still unchanged in an omnidirectional image, and the laser scan projected onto the omnidirectional image, because local and global features can be extracted from this data fusion [20]. An important tool for doing this is the extrinsic calibration described in this work, applied to omnidirectional images and laser scans taken without calibration patterns. Fig. 9 shows how the depth information provided by the LRF is projected onto the omnidirectional image, and how the corners match with the scene vertical lines. A good example of this is the heater on the wall, and the wall corner just below. Fig. 10 shows not only the depth information on the omnidirectional image, but

part of a place with a wall distribution different from typical square rooms. Note the visible match between the contour of the laser and the image of the place. In the case of Fig. 9 and 10, we did not a pixel error comparison since we were not allowed to get a ground truth data.

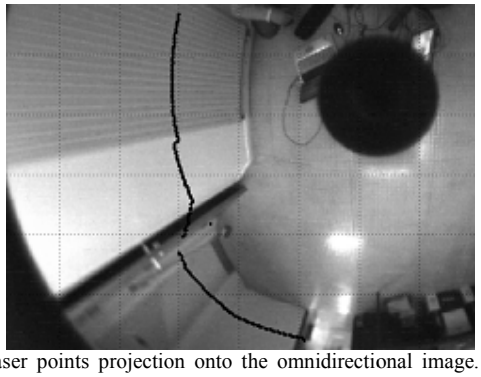

Fig. 9. Laser points projection onto the omnidirectional image. Note the depth difference in the image of the heater on the wall.

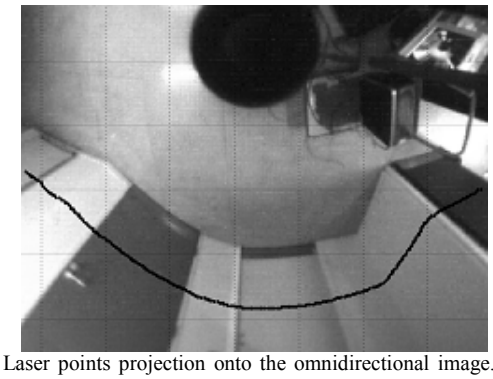

Fig. 10. Laser points projection onto the omnidirectional image. Note the visible match between the contour of the laser and the image of the place.

V. CONCLUSION

Embedding range information in omnidirectional images has been achieved using two proposed methods to perform an extrinsic calibration between an LRF with an invisible laser trace and a catadioptric camera. LRF calibration was also been performed, getting practical and interesting characteristics such as the warm-up period and the LRF model. The two methods proposed require the calibration checkerboard patterns to be visible to both the LRF and the catadioptric camera. For both methods, the catadioptric camera's intrinsic parameters are used to impose a non-linear minimization function based on geometrical constraints and solved using the LM algorithm. Three different versions of initial guesses for the LM algorithm were presented, and their rank-2 problem resolved. The first method proposed simultaneously estimates the extrinsic parameters and performs a second minimization step based on the MSE of all the calibration poses. This method performs a 6DOF estimation, which may be noisy and it requires more training data. The second method performs a non-simultaneous estimation. First the translation vector is estimated and then the rotation matrix is found. This method performs two 3DOF estimations, which requires less training data and less noise is involved. Therefore, we think the first method is better if enough data is available, even though it has shown more accurate results in some cases; and we think in the second method is more likely to get a calibration result. Unlike other approaches, the methods proposed here are evaluated at pixel error level using ground truth data from the calibration patterns and projected onto the omnidirectional image, which is important information for data fusion approaches. This kind of calibration is very useful for mobile robotics appearance-based mapping, localization and navigation, data fusion approaches, and local navigation through potential field strategies.

REFERENCES

[1] S. Wasielewski and O. Strauss, "Calibration of a multi-sensor system laser rangefinder/camera", Proc. of the Int. Vehic. pp. 472–477, 1995.

[2] Q. Zhang and R. Pless, "Constraints for Heterogeneous Sensor Auto-Calibration", in Proc. IEEE Workshop on Real Time 3D Sensors and Their Use, 2004.

[3] Q. Zhang and R. Pless, Extrinsic Calibration of a Camera and Laser Range Finder (improves camera intrinsic calibration), in Proc. of IEEE Intl. Conference on Intelligent Robots and Systems, (2004).

[4] M. Antone, and Y. Friedman, "Fully Automated Laser Range Calibration", BMVC07, (2007).

[5] C. Mei and P. Rives. Calibration between a Central Catadioptric Camera and a Laser Range Finder for Robotic Applications, In Proceedings of ICRA'06, Orlando, May, (2006).

[6] R. Unnikrishnan and M. Hebert, "Fast Extrinsic Calibration of a Laser Rangefinder to a Camera," tech. report CMU-RI-TR-05-09, Robotics Institute, Carnegie Mellon University, July, 2005.

[7] D. Scaramuzza, A. Harati and R. Siegwart. Extrinsic self calibration of a camera and a 3D laser range finder from natural scenes. IEEE 2007.

[8] Y. Soo-Yeong; C. Byoung-Wook; N. Ahuja, "Real-time Omni-directional Distance Measurement with Active Panoramic Vision", Int. Jour. of Ctrl., Aut., and Sys., v5, no.2, pp.184-191, 2007.

[9] O. Radu J. Salvi, E. Mouaddib, "Calibration of A Structured Light-Based Stereo Catadioptric Sensor", Comp. Vis. and Patt. Recog. Workshop, 2003. Conf. on, 16-22 2003.

[10] J. Weingarten, Feature-based 3D SLAM. PhD Thesis, Swiss Federal Institute of Technology Lausanne, EPFL, no 3601, Dir.: Roland Siegwart, (2006).

[11] C. Mei, Calibration Toolbox for omnidirectional cameras. http://www.robots.ox.ac.uk/~cmei/Toolbox.html.

[12] Reina and J. Gonzalez, "Characterization of a radial laser scanner for mobile robotic navigation,"Proc. IEEE/RSJ Int. Conf. on Intelligent robots and systems, pp. 579-585, 1997.

[13] C. Ye, and J. Borenstein, "Characterization of a 2-D Laser Scanner for Mobile Robot Obstacle Negotiation," Proc. IEEE Int. Conf. on Robotics and Automation, 2512-2518 (2002).

[14] Y. Okubo, C. Ye, and J. Borenstein, "Characterization of the Hokuyo URG-04LX Laser Rangefinder for Mobile Robot Obstacle Negotiation." SPIE Def., Sec.+Sens.; Unmanned Sys. Tech. XI, Conf. 7332: Unmanned, Robotic, and Layered Systems, 2009.

[15] C. Geyer and K. Daniilidis. "A unifying theory for central panoramic systems and practical implications". In ECCV, 2000.

[16] J. Barreto and A. Helder, "Issues on the geometry of central catadioptric image formation". In CVPR, 2001.

[17] C. Mei and P. Rives, "Single View Point Omnidirectional Camera Calibration from Planar Grids", IEEE Int.Conf.on Rob.and Aut., 2007.

[18] K. Madsen, H. Nielsen, O. Tingleff, "Methods for Non-Linear Least Squares Problems", Inf.and Math. Model., Technical University of Denmark, 2nd Edition, 2004.

[19] D. Eggert, D. A. Lorusso, and R. Fisher, Estimating 3-D rigid body transformations: a comparison of four major algorithms. Mach. Vision Appl. 9, 5-6 1997.

[20] B. Bacca, J. Salvi, and X. Cufi, Appearance-Based SLAM for Mobile Robots. In Proc. of Conf. on Artificial intell. Research and Development, Frontiers in Artificial Intelligence and Applications, vol. 202. IOS Press, Amsterdam, The Netherlands, 55-64, 2009.